

# Higher order accuracy in the gap-tooth scheme for large-scale solutions using microscopic simulators

A. J. Roberts\*      I. G. Kevrekedis†

September 20, 2004

## Abstract

We discuss a framework for multiscale computation which enables models at a “microscopic” level of description, for example Lattice Boltzmann, Monte Carlo or Molecular Dynamics simulators, to perform modelling tasks at the “macroscopic” length scales of interest. This macroscopic modeling task is accomplished through microscopic simulations over only small spatial domains. In contrast, traditional spatio-temporal modeling first involve the derivation of macroscopic evolution equations, usually using some heuristic closure; then analytical and numerical techniques solve the resultant partial differential equations. Our approach can bypass the derivation of the macroscopic evolution equations. We use instead the microscopic rules themselves, but restricted to small parts of the domain, the “teeth”, followed by interpolation to estimate macroscopic fields in the “gaps”. The challenge addressed here is to find general boundary conditions for the microscopic simulators that appropriately connect the widely separated “teeth” to achieve high order accuracy over the macroscale. Here we start by exploring the issues in the simplest case of random walkers in one-dimension. For this case the diffusion equation applies on both macroscopic and microscopic length scales, and analytic solutions provide comparisons. The internal boundary conditions of holistic discretisation adapt to the small isolated patches of

---

\*Dept. Maths & Computing, University of Southern Queensland, Toowoomba, AUSTRALIA. <mailto:aroberts@usq.edu.au>

†Program in Applied and Computational Mathematics, Princeton University, Princeton, NJ 08544, USA. <mailto:yannis@Princeton.edu>

the spatial domain that form the “teeth”. We show this achieves arbitrarily high-order consistency in the gap-tooth scheme, and with care are numerically stable. When applied to other microscopic simulators we should achieve efficient large scale simulation using only relatively sparse microscopic simulations.

## Contents

<b>1</b>	<b>Introduction</b>	<b>2</b>
<b>2</b>	<b>Couple the patches</b>	<b>5</b>
<b>3</b>	<b>Achieve high order consistency</b>	<b>6</b>
<b>4</b>	<b>Diffusive model is numerically stable</b>	<b>9</b>
<b>5</b>	<b>Conclusion</b>	<b>11</b>
	<b>References</b>	<b>12</b>

## 1 Introduction

As a preliminary illustration of the gap-tooth scheme [5, 12, 13], consider simulating the diffusion and nonlinear advection of Burgers’ equation

$$\frac{\partial u}{\partial t} + 100u \frac{\partial u}{\partial x} = \frac{\partial^2 u}{\partial x^2}. \quad (1)$$

Suppose our aim is to simulate the evolution of fields  $u(x, t)$  periodic in  $x$  on the macroscopic length scale  $2\pi$ . See in Figure 1 the continuous time evolution on  $m = 8$  grid “points” in space with the macroscopic spacing  $H = \pi/4$ . However, each “point” is actually a microscopic patch of size  $h = \pi/20$ . Further, the *only* knowledge that the macroscopic evolution has of Burgers’ equation (1) is through the microscopic simulation within each patch; here we obtain this microscopic simulation via a discretisation on a microscopic spatial grid of  $n = 11$  points within each patch,  $\Delta x = 0.0175$ , and on a microscopic time step of  $\Delta t \approx 10^{-4}$ . This microscopic discretisation of Burgers’ equation (1) represents a fine detailed model or particle simulation

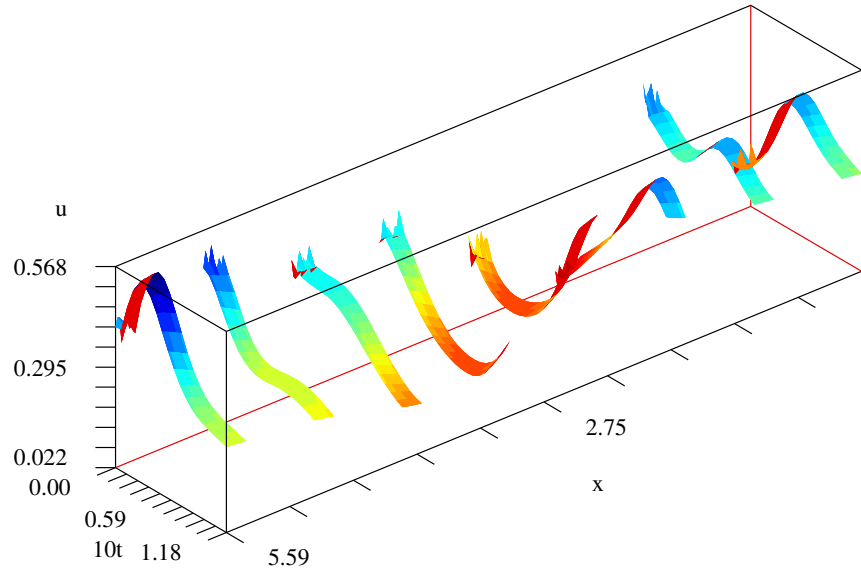


Figure 1: Gap-tooth solution of Burgers' equation (1) on  $[0, 2\pi]$  through microsimulation on 8 patches each of small length  $\pi/20$  and the patches coupled by special boundary conditions.

that is too expensive to use over the entire macroscopic domain. Our task here is to begin to show how such microscopic simulations in *relatively small* patches of space may be coupled by patch boundary conditions derived in Section 2 to ensure high order accuracy over the macroscopic domain.

In the example shown in Figures 1 and 2 see that there are two time scales in the simulation. Rapidly, the initial internal structure within each patch (black curves in Figure 2) smooths by diffusion on the microscopic time-scale to a microscopic quasi-equilibrium (blue curves). Then over macroscopic times the inter-patch coupling exchanges information between the patches to guide how the microscopic quasi-equilibria evolves over macroscopic times. See in Figure 2: the nonlinear advection to the right of the hump that is initially centred around  $x \approx 3$  but at the end is centred about  $x \approx 5$  (red curves); whereas the short hump at  $x \approx 0$  is dissipated more quickly to be only a small hump at  $x \approx 1$  at the end of the macroscopic simulation. Because of the two time scales, we plan future research to implement “coarse grained” integration [3, 4] which uses just short bursts of microscopic integration to then extrapolate over a macroscopic time step. The result will then be a scheme where the microscopic simulations are only needed for relatively small patches in space-time. However, here we concentrate on only the issue of the

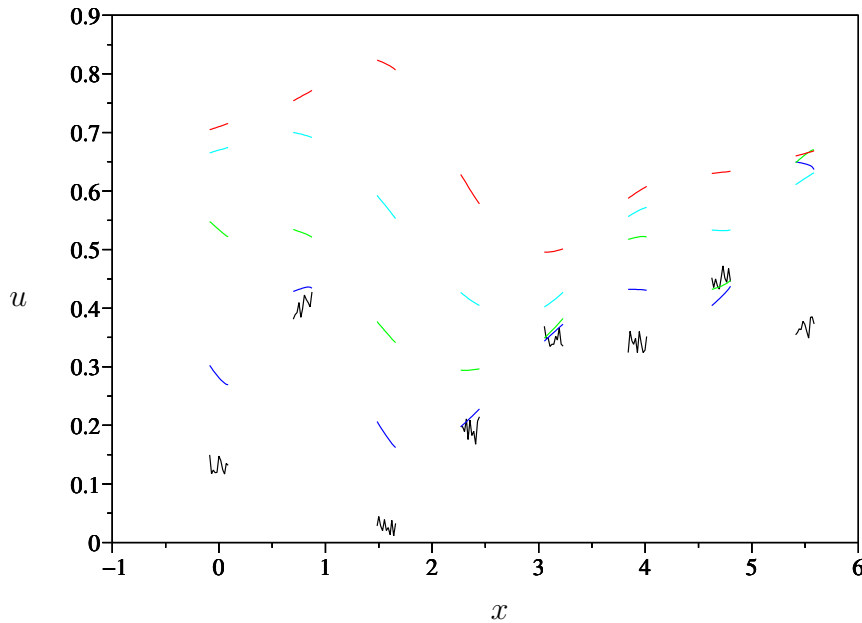


Figure 2: Gap-tooth solution of Burgers' equation (1) on  $[0, 2\pi]$  through microsimulation on 8 patches each of small length  $\pi/20$  and the patches coupled by special boundary conditions. Solutions  $u(x, t) + 4t$  are plotted at five times  $t = 0 : 0.025 : 0.1$  in different colours and with the vertical displacement of  $4t$  to help distinguish the plots.

macroscopic coupling of small patches in space.

The method of “holistic discretisation”, developed by Roberts and Mackenzie [9, 10, 11, 6], creates discretisations on a macroscopic grid using systematic analytic approximations for the subgrid field. The analytic solutions obtained in Section 3 using this method are analogous to the microscopic system simulators in the gap-tooth scheme: they both provide microscopic solutions to be macroscopically coupled to neighbouring elements. This dynamical systems approach uses adapted versions of the patch boundary conditions to support the modelling by centre manifold theory [10]. Then the equivalent PDE of the macroscopic dynamic model is found, in Section 3, to confirm the high order consistency for a wide class of linear PDEs.

Lastly, in Section 4, we consider a numerical time integrator for the diffusion equation on patches. The eigenvalues of the integrator again confirm the high order accuracy of the proposed patch boundary conditions.

## 2 Couple the patches

In this section we develop a coupling of the internal dynamics of patches with their neighbours to achieve high order consistency. Here we require a boundary condition for the flux on the edge of the microscopic patches that is a natural interpolation of the surrounding macroscopic field.

We introduce the notation in which we typically use capital letters for macroscopic quantities and lower case letters for microscopic quantities. Thus let each of  $m$  patches be centred on equi-spaced grid points  $x = X_j = jH$  seen in Figures 1 and 2. Let each patch be of width  $h$ . Then the edge of a patch is a distance  $h/2$  from its grid point, a fraction  $r = h/(2H)$  to the neighbouring grid point: when  $r = \frac{1}{2}$  the neighbouring patches meet and there would be no gap, as in holistic discretisation [9]. Here we expect the fraction  $r$  to be small so that the patches are a relatively small part of the physical domain. For example,  $r = 1/10$  in Figures 1 and 2. Now let  $v_j(x, t)$  be the microscopic field in the  $j$ th patch.

We use the following identities for discrete operators [7] on a step size of the macroscopic grid and be careful whether we are using as a step of  $H$  in  $x$  or a step of 1 in  $j$ . In terms of the shift operator,  $Ev(x, t) = v(x + H, t)$  or equivalently  $EU_j = U_{j+1}$ :

$$\text{centred mean} \quad \mu = \frac{1}{2}(E^{1/2} + E^{-1/2}), \quad (2)$$

$$\text{centred difference} \quad \delta = E^{1/2} - E^{-1/2}, \quad (3)$$

$$\text{translate/shift} \quad E = 1 + \mu\delta + \frac{1}{2}\delta^2, \quad (4)$$

$$\text{derivative in } x \quad H\partial_x = 2 \sinh^{-1} \frac{1}{2}\delta, \quad (5)$$

$$\text{an identity} \quad \mu^2 = 1 + \frac{1}{4}\delta^2. \quad (6)$$

For example, the derivative of the microscopic field on the edge of a patch,  $H \frac{\partial v_j}{\partial x}$  at  $(X_j \pm rH, t)$ , may be obtained from  $v_j$  through applying the operator

$$\begin{aligned} E^{\pm r} H \partial_x &= (1 + \mu\delta + \frac{1}{2}\delta^2)^{\pm r} 2 \sinh^{-1} \frac{1}{2}\delta \quad \text{by (4) and (5)} \\ &= [1 \pm r\mu\delta + \mathcal{O}(\delta^2)][\delta + \mathcal{O}(\delta^3)] \\ &= \delta \pm r\mu\delta^2 + \mathcal{O}(\delta^3) \\ &= \mu\delta \pm r\delta^2 + \mathcal{O}(\delta^3) \quad \text{by (6)}. \end{aligned} \quad (7)$$

This last operator just involves evaluation at the grid points  $X_j$  and hence is evaluated from the macroscopic grid values  $U_j$ . This is the same approximation for the microscopic gradient as obtained by quadratic interpolation through the neighbouring macroscopic grid values [5, e.g.]. We proceed to

modify such a patch boundary condition in order to obtain higher order consistency with the surrounding macroscopic variations.

For arbitrary order consistency, as macroscopic grid size  $H \rightarrow 0$  or as the gradients become small, repeat the previous analysis but retain more terms, and using (6) to replace  $\mu^2$  terms:

$$\begin{aligned}
E^{\pm r} H \partial_x &= (1 + \mu\delta + \frac{1}{2}\delta^2)^{\pm r} 2 \sinh^{-1} \frac{1}{2}\delta \\
&= \frac{\mu}{\sqrt{1 + \frac{1}{4}\delta^2}} (1 + \mu\delta + \frac{1}{2}\delta^2)^{\pm r} 2 \sinh^{-1} \frac{1}{2}\delta \\
&= \mu\delta \pm r\delta^2 - (\frac{1}{6} - \frac{1}{2}r^2)\mu\delta^3 \mp r(\frac{1}{12} - \frac{1}{6}r^2)\delta^4 \\
&\quad + (\frac{1}{30} - \frac{1}{8}r^2 + \frac{1}{24}r^4)\mu\delta^5 \pm r(\frac{1}{90} - \frac{1}{36}r^2 + \frac{1}{120}r^4)\delta^6 \\
&\quad - (\frac{1}{140} - \frac{7}{240}r^2 + \frac{1}{72}r^4 - \frac{1}{720}r^6)\mu\delta^7 \\
&\quad \mp r(\frac{1}{560} - \frac{7}{1440}r^2 + \frac{1}{480}r^4 - \frac{1}{5040}r^6)\delta^8 + \mathcal{O}(\delta^9). \tag{8}
\end{aligned}$$

Numerical eigenanalysis of the diffusion equation (16) reported in Section 4 confirms the high order accuracy and stability of the resultant integration scheme with patch boundary conditions from the above operator.

### 3 Achieve high order consistency

Here we demonstrate analytically that appropriate patch boundary conditions achieve high order consistency for a wide class of PDEs. Consider the linear PDE

$$\frac{\partial u}{\partial t} = \frac{\partial^2 u}{\partial x^2} - c \frac{\partial u}{\partial x} - b \frac{\partial^3 u}{\partial x^3} - a \frac{\partial^4 u}{\partial x^4}, \tag{9}$$

for some constants  $a$ ,  $b$  and  $c$ —we have chosen time and space scales so that the coefficient of the diffusion term is 1. Specific boundary conditions on small patches ensures macroscopic consistency.

Following the dynamical systems approach of holistic discretisation [9, 10] we introduce the parameter  $\gamma$  to control the coupling between patches: when  $\gamma = 0$  the patches are uncoupled to form a base for us to apply centre manifold theory; but when we consequently set  $\gamma = 1$  we recover a dynamical model for the original PDE. Modify the operator (8) to invoke the patch boundary condition (PBC) that on  $x = X_j$  (noting that the  $E^{\pm r}$  implies the left-hand side is evaluated on the edge of the patch at  $x = X_j \pm rH$ ):

$$\begin{aligned}
E^{\pm r} H \partial_x v_j &= \left\{ \gamma [\mu\delta \pm r\delta^2] + \gamma^2 [-(\frac{1}{6} - \frac{1}{2}r^2)\mu\delta^3 \mp r(\frac{1}{12} - \frac{1}{6}r^2)\delta^4] \right. \\
&\quad \left. + \gamma^3 [+(\frac{1}{30} - \frac{1}{8}r^2 + \frac{1}{24}r^4)\mu\delta^5 \pm r(\frac{1}{90} - \frac{1}{36}r^2 + \frac{1}{120}r^4)\delta^6] \right\}
\end{aligned}$$

$$+ \gamma^4 \left[ -\left(\frac{1}{140} - \frac{7}{240}r^2 + \frac{1}{72}r^4 - \frac{1}{720}r^6\right)\mu\delta^7 \mp r\left(\frac{1}{560} - \frac{7}{1440}r^2 + \frac{1}{480}r^4 - \frac{1}{5040}r^6\right)\delta^8 \right] \} U_j. \quad (10)$$

See in the PBC that when  $\gamma = 0$  the small patches are decoupled and the insulating PBCs,  $E^{\pm r} \partial_x v_j = 0$ , cause the dissipative dynamics of (9) in each patch to decay exponentially quickly to some constant field in each patch, namely  $v_j(x, t) \rightarrow U_j$  for each of the  $m$  patches. For non-zero coupling parameter  $\gamma$  the subgrid scale patch field is no longer constant, and each patch grid value  $U_j$  evolves because of the coupling with its neighbours. We construct a series solution of the PDE (9) in the coupling parameter  $\gamma$ : the first order expression for the microscopic subgrid scale field is straightforward, namely

$$v_j = U_j + \gamma \left( \xi\mu\delta + \frac{1}{2}\xi^2\delta^2 \right) U_j + c\gamma H \left( -\frac{1}{2}r^2\xi + \frac{1}{6}\xi^3 \right) \delta^2 U_j + \mathcal{O}(\gamma^2, a^2 + b^2 + c^2), \quad (11)$$

where the microscopic variable  $\xi = (x - X_j)/H$  ranges over  $|\xi| < r$ ; accompanying these subgrid fields the grid values  $U_j$  evolve according to standard second order discretisation (upon putting  $\gamma = 1$ )

$$\dot{U}_j = \gamma \left( \frac{1}{H^2} \delta^2 U_j - \frac{c}{H} \mu \delta U_j \right) + \mathcal{O}(\gamma^2, a^2 + b^2 + c^2). \quad (12)$$

See that the powers of the coupling parameter  $\gamma$  in the PBC (10) are chosen so that discarding terms of  $\mathcal{O}(\gamma^p)$  results in a discrete model, such as (12), which is of width  $2p - 1$  in the grid values  $U_j$ ; for example, the above model only involves  $U_j$  and  $U_{j\pm 1}$ . Centre manifold theory [1, 2, e.g.] asserts that for small enough  $\gamma$  the resulting model is exponentially quickly attractive and faithfully models the dynamics of the system. Although no proof is yet available, we anticipate that the case of interest, when  $\gamma = 1$ , is small enough for this novel theoretical support to still hold.

In the interim we demonstrate high order consistency. Obtain models that resolve more detail of the subgrid microscopic dynamics and its interaction with neighbouring patches by determining higher order terms in the coupling parameter  $\gamma$ . Iteration [8] straightforwardly generates higher order approximations.<sup>1</sup> For example, discarding terms  $\mathcal{O}(\gamma^3)$  the subgrid field in each patch is modified from (11) to

$$v_j = \left\{ 1 + \gamma \left[ \xi\mu\delta + \frac{1}{2}\xi^2\delta^2 \right] + \gamma^2 \left[ \frac{1}{6}(\xi^3 - \xi)\mu\delta^3 + \frac{1}{24}(\xi^2 - \xi^4)\delta^4 \right] \right.$$

<sup>1</sup>We use the REDUCE computer algebra package which has free demonstration versions available via <http://reduce-algebra.com>. Obtain our code for this problem from <http://www.sci.usq.edu.au/staff/aroberts/linpbc.red>.

$$\begin{aligned}
& + cH \left[ (\gamma - \gamma^2) \frac{1}{6} \xi^3 \delta^2 + \gamma^2 \left( \frac{1}{60} \xi^5 - \frac{1}{18} \xi^3 \right) \delta^4 \right] + \frac{b}{H} \gamma^2 \frac{1}{6} \xi^3 \delta^4 \\
& + r^2 \left[ -cH (\gamma - \gamma^2) \frac{1}{2} \xi \delta^2 - cH \gamma^2 \left( \frac{1}{12} \xi^3 - \frac{1}{6} \xi \right) \delta^4 - \frac{b}{H} \gamma^2 \frac{1}{2} \xi \delta^4 \right] \\
& + r^4 cH \frac{1}{6} \xi \delta^4 \left. \right\} U_j + \mathcal{O}(\gamma^3, a^2 + b^2 + c^2). \tag{13}
\end{aligned}$$

The first line in (13) is the leading few terms in a universal subgrid structure for symmetric operators. However, odd operators, such as the advection  $c \frac{\partial u}{\partial x}$  and the dispersion  $b \frac{\partial^3 u}{\partial x^3}$ , generate nontrivial subgrid structures in each patch, such as those in the second line of (13), which reflect subgrid scale interaction of processes. The third and fourth line of the approximate field (13) depend upon the patch size  $r = h/(2H)$ . But physically the subgrid scale field in each patch should be independent of the patch size  $r$ . Although there is some dependence in these approximations, higher orders in the coupling parameter  $\gamma$  remove it. For example, at the beginning of the third line in (13) see the term  $-cH(\gamma - \gamma^2) \frac{1}{2} \xi \delta^2$  disappears when we set  $\gamma = 1$  for the physically relevant approximation. Similarly, computing the next order terms in coupling parameter  $\gamma$  generates terms, in  $\gamma^3$ , which cancel the  $r$  dependent terms in the third and fourth line of the subgrid field (13). Thus higher order models push any undesirable  $r$  dependence to higher orders, thereby usefully predicting a subgrid field largely independent of the patch size  $r$ .

Simultaneously with the derivation of the subgrid field (13) we determine the corresponding evolution of the macroscopic grid values  $U_j$  for the PDE (9). Compute to higher order in coupling parameter  $\gamma$  obtain refinements to the basic discretisation (12); for example, here we discard terms  $\mathcal{O}(\gamma^4)$  to determine

$$\begin{aligned}
\dot{U}_j & = \frac{1}{H^2} \left( \gamma \delta^2 - \frac{1}{12} \gamma^2 \delta^4 + \frac{1}{90} \gamma^3 \delta^6 \right) U_j - \frac{c}{H} \left( \gamma \mu \delta - \frac{1}{6} \gamma^2 \mu \delta^3 + \frac{1}{30} \gamma^3 \mu \delta^5 \right) U_j \\
& - \frac{b}{H^3} \left( \gamma^2 \mu \delta^3 - \frac{1}{4} \gamma^3 \mu \delta^5 \right) U_j - \frac{a}{H^4} \left( \gamma^2 \delta^4 - \frac{1}{6} \gamma^3 \delta^6 \right) U_j \\
& + \mathcal{O}(\gamma^4, a^2 + b^2 + c^2). \tag{14}
\end{aligned}$$

Set  $\gamma = 1$  to recover a model for the PDE (9) supported by centre manifold theory. Note how truncating the expansion to different powers of coupling parameter  $\gamma$  changes the width in  $U_j$  of the discrete model. With the patch boundary conditions (10) the model is independent of the patch size  $r$ .

As well as the novel dynamical systems support, another way to assess the model's relevance is to compare the original PDE with the equivalent PDE obtained from model (14) in the limit as the macroscopic spacing  $H \rightarrow 0$ .

From (14), straightforward algebra<sup>2</sup> deduces the equivalent PDE

$$\begin{aligned} \frac{\partial U}{\partial t} = & \gamma \frac{\partial^2 U}{\partial x^2} - \gamma c \frac{\partial U}{\partial x} - \gamma^2 b \frac{\partial^2 U}{\partial x^2} - \gamma^2 a \frac{\partial^4 U}{\partial x^4} \\ & + H^2 \left[ (\gamma - \gamma^2) \left( \frac{1}{12} \frac{\partial^4 U}{\partial x^4} - \frac{1}{6} c \frac{\partial^3 U}{\partial x^3} \right) - (\gamma^2 - \gamma^3) \left( \frac{1}{4} b \frac{\partial^5 U}{\partial x^5} + \frac{1}{6} a \frac{\partial^6 U}{\partial x^6} \right) \right] \\ & + H^4 \left[ \left( \frac{1}{360} \gamma - \frac{1}{72} \gamma^2 + \frac{1}{90} \gamma^3 \right) \left( \frac{\partial^6 U}{\partial x^6} - 3c \frac{\partial^5 U}{\partial x^5} \right) \right. \\ & \left. - \left( \frac{1}{80} \gamma^2 - \frac{1}{24} \gamma^3 \right) \left( b \frac{\partial^7 U}{\partial x^7} + 2a \frac{\partial^8 U}{\partial x^8} \right) \right] + \mathcal{O}(H^6, \gamma^4, a^2 + b^2 + c^2). \quad (15) \end{aligned}$$

Set coupling parameter  $\gamma = 1$ , then the second and third lines in the equivalent PDE (15) disappear and consequently the diffusion and advection is modelled with errors of  $\mathcal{O}(H^6)$ , whereas the dispersion and the fourth-order dissipation is modelled with errors  $\mathcal{O}(H^4)$ . Should you truncate the discretisation (14) to lower orders in coupling parameter  $\gamma$ , there is less cancellation in the equivalent PDE and the errors are consequently larger. Conversely, the errors move to progressively higher orders as more terms in the coupling parameter  $\gamma$  are retained in the centre manifold discretisation (14). Our patch boundary conditions (10) seem to create excellent discretisations for PDEs.

## 4 Diffusive model is numerically stable

Although the PBCs (10) are consistent we need to confirm they are numerically stable. Indeed many other forms of PBCs were tried before finding one that was both consistent and numerically stable. In this section we explore the gap-tooth simulations of the simple diffusion equation

$$\frac{\partial u}{\partial t} = \frac{\partial^2 u}{\partial x^2}, \quad \text{and } 2\pi\text{-periodic in } x. \quad (16)$$

Imagine we only have access to the dynamics through a microscopic simulator of the diffusion (16), here coded by a microscopic discretisation on  $n$  grid points in a patch of microscopic size  $h = rH$  and with some microscopic time step, typically  $\Delta t = 10^{-6}$ – $10^{-4}$ .

First we implement the PBC that on the edge of each patch, at  $x = X_j \pm rH$ , the microscopic discretisation has boundary condition

$$H \partial_x v_j = \left[ \mu \delta \pm r \delta^2 - \left( \frac{1}{6} - \frac{1}{2} r^2 \right) \mu \delta^3 \mp r \left( \frac{1}{12} - \frac{1}{6} r^2 \right) \delta^4 \right] U_j. \quad (17)$$

<sup>2</sup>See our REDUCE code from the internet.

Table 1: Growth rates  $\lambda$  of perturbations from steady state  $u = 0$ : for diffusion (16) with  $m$  patches; with gap to patch ratio  $r = 0.1$ ;  $n = 11$  points in the microscale grid; and with fourth order PBC (17).

$m$	1	2,3	4,5	6,7	$m + 1 : 2m$
4	$2 \times 10^{-12}$	-0.946817	-2.170942	n/a	-99.79
8	$5 \times 10^{-12}$	-0.996139	-3.787268	-7.132829	-399.1
16	$2 \times 10^{-10}$	-0.999758	-3.984556	-8.834269	-1596.
32	$-2 \times 10^{-10}$	-0.999987	-3.999031	-8.988851	-6386.

Table 2: Growth rates of perturbations from steady state  $u = 0$  as for Table 1 but fewer points in the microscale grid, namely  $n = 7$ .

$m$	1	2,3	4,5	6,7	$m + 1 : 2m$
4	$8 \times 10^{-13}$	-0.947206	-2.173003	n/a	-99.30
8	$-8 \times 10^{-12}$	-0.996246	-3.788826	-7.138379	-397.2
16	$-1 \times 10^{-11}$	-0.999785	-3.984985	-8.836383	-1588.
32	$8 \times 10^{-11}$	-0.999994	-3.999139	-8.989397	-6355.

Obtain this from the first few terms of (8) or equivalently from PBC (10) by discarding  $\mathcal{O}(\gamma^3)$  terms. For the  $j$ th patch this PBC involves macroscopic grid values  $U_{j-2}, \dots, U_{j+2}$  only. Then systematically perturbing each and every microscopic value from zero, there are  $mn$  such microscopic values, we numerically determined the map of one microscopic time step. Transform the eigenvalues  $\mu$  of this map to growth rates  $\lambda = \log(\mu)/\Delta t$ . The  $mn$  growth rates fall into  $n$  groups of  $m$  modes. Each group roughly corresponds to a microscopic internal mode of the dynamics, roughly  $\exp(\lambda_\ell t) \cos[\ell\pi(x - X_j + h/2)/h]$  for growth rate  $\lambda_\ell \approx -\ell^2\pi^2/h^2$  for  $\ell = 0, 1, \dots, n-1$ . For  $\ell \geq 1$  these are the rapidly decaying microscopic modes internal to each patch seen in the initial instants of the simulations of Figures 1 and 2. The other group of  $m$  modes,  $\ell = 0$ , with small growth rates, correspond to the slowly evolving macroscopic modes of interest that arise through the coupling between patches of the microscopic dynamics. Table 1 shows the leading seven growth rates, and the magnitude of the  $\ell = 1$  internal growth rates, for various numbers of patches,  $m = 4, 8, 16, 32$ . The exact growth rates of the diffusion PDE (16) are  $\lambda = -k^2$  for integer  $k$ . See in the table that as the number of patches double, the accuracy of the growth rates of the macroscopic modes improves by a factor of about 16. This is consistent with an  $\mathcal{O}(H^4)$  method as predicted for diffusion with PBC (17).

Second, we repeat the analysis for fewer subgrid scale points so that the microscopic dynamics are not resolved as well. Table 2 shows the leading

Table 3: Growth rates of perturbations from steady state  $u = 0$  as for Table 1 but with the sixth order PBC (18).

$m$	1	2,3	4,5	6,7	$m + 1 : 2m$
4	$8 \times 10^{-12}$	-0.982238	-2.457648	n/a	-99.79
8	$4 \times 10^{-11}$	-0.999677	-3.928952	-7.843254	-399.1
16	$4 \times 10^{-11}$	-1.000006	-3.998708	-8.967122	-1596.
32	$-2 \times 10^{-10}$	-1.000003	-4.000023	-8.999625	-6386.

eigenvalues for  $n = 7$  points in each patch. There is no significant difference between Tables 1 and 2 indicating that the microscopic resolution, the only difference between the two, has little impact on the macroscopic dynamics. No growth rate is significantly positive showing the numerical method is stable—the leading growth rate is close to zero corresponding to conservation of material. The other dominant growth rates rapidly approach those for diffusion.

Lastly, consider the diffusive dynamics of (16) when connected by the PBC that at  $x = X_j \pm rH$

$$H\partial_x v_j = \left[ \mu\delta \pm r\delta^2 - \left(\frac{1}{6} - \frac{1}{2}r^2\right)\mu\delta^3 \mp r\left(\frac{1}{12} - \frac{1}{6}r^2\right)\delta^4 + \left(\frac{1}{30} - \frac{1}{8}r^2 + \frac{1}{24}r^4\right)\mu\delta^5 \pm r\left(\frac{1}{90} - \frac{1}{36}r^2 + \frac{1}{120}r^4\right)\delta^6 \right] U_j. \quad (18)$$

Obtain this PBC from the first six terms of (8) or equivalently from PBC (10) by discarding  $\mathcal{O}(\gamma^4)$  terms. Table 3 demonstrates that the resultant numerical scheme is stable and has sixth order consistency for the diffusion equation. Further, it is these PBCs we used to simulate the nonlinear dynamics of Burgers' equation (1) to create Figures 1 and 2.

## 5 Conclusion

We achieve higher order accuracy in the gap-tooth scheme using carefully crafted patch boundary conditions (PBCs). Analytic approximations and analysis of numerical steps in time confirm the PBCs (17) and (18) are effective. Importantly the PBCs (17) and (18) do *not* depend upon the particular PDE being simulated, thus the PBCs should work effectively for particle simulations for which we do not have a microscale closure.

Further, although the predicted microscopic subgrid scale fields do have some dependence upon the patch size  $r$ , the dependence is weakens, by being pushed to higher orders in  $r$ , in using higher order accuracy patch boundary conditions.

As shown in Figures 1 and 2, the PBCs we have implemented here appear to work well even for the nonlinear advection of Burgers equation (1).

## References

- [1] J. Carr. *Applications of centre manifold theory*, volume 35 of *Applied Math. Sci.* Springer-Verlag, 1981. 7
- [2] J. Carr and R. G. Muncaster. The application of centre manifold theory to amplitude expansions. II. Infinite dimensional problems. *J. Diff. Eqns*, 50:280–288, 1983. 7
- [3] Jaime Cisternas, C. William Gear, Simon Levin, and Ioannis G. Kevrekidis. Equation-free modeling of evolving diseases: Coarse-grained computations with individual-based models. Technical report, [<http://arXiv.org/abs/nlin.A0/0310011>], 2003. 3
- [4] C. William Gear, Ioannis Kevrekidis, and Constantinos Theodoropoulos. ‘coarse’ integration/bifurcation analysis via microscopic simulators: micro-galerkin methods. *Computers and Chemical Engrg*, 26:941–963, 2002. 3
- [5] C. William Gear, Ju Li, and Ioannis G. Kevrekidis. The gap-tooth method in particle simulations. *Phys. Lett. A*, 316:190–195, 2003. 2, 5
- [6] T. MacKenzie and A. J. Roberts. Holistic discretisation of shear dispersion in a two-dimensional channel. In K. Burrage and Roger B. Sidje, editors, *Proc. of 10th Computational Techniques and Applications Conference CTAC-2001*, volume 44, pages C512–C530, March 2003. <http://anziamj.austms.org.au/V44/CTAC2001/Mack>. 4
- [7] National Physical Laboratory. *Modern Computing Methods*, volume 16 of *Notes on Applied Science*. Her Majesty’s Stationary Office, 1961. 5
- [8] A. J. Roberts. Low-dimensional modelling of dynamics via computer algebra. *Computer Phys. Comm.*, 100:215–230, 1997. 7
- [9] A. J. Roberts. Holistic discretisation ensures fidelity to Burgers’ equation. *Applied Numerical Modelling*, 37:371–396, 2001. 4, 5, 6
- [10] A. J. Roberts. A holistic finite difference approach models linear dynamics consistently. *Mathematics of Computation*, 72:247–262, 2002. 4, 6

- [11] A. J. Roberts. A step towards holistic discretisation of stochastic partial differential equations. In Jagoda Crawford and A. J. Roberts, editors, *Proc. of 11th Computational Techniques and Applications Conference CTAC-2003*, volume 45, pages C1–C15, December 2003. [Online] <http://anziamj.austms.org.au/V45/CTAC2003/Robe/home.html> [December 14, 2003]. 4
- [12] Giovanni Samaey, Ioannis G. Kevrekidis, and Dirk Roose. Damping factors for the gap-tooth scheme. Technical report, Princeton University, November 2003. 2
- [13] Giovanni Samaey, Ioannis G. Kevrekidis, and Dirk Roose. The gap-tooth scheme for homogenization problems. Technical report, Princeton University, October 2003. 2